from ^{87}Rb signals. Qualitatively, the results are similar to the cesium results. There are two features worth pointing out. First, the polarizabilities are smaller. Second, Eq. (12) is much better satisfied than in the case of cesium. This corresponds to the fact that the spin-orbit splitting in rubidium is much smaller than in cesium. In Table II the measured polarizabilities are compared with calculations based on the Bates-Damgaard method. Agreement here is also excellent.

The electric field was taken from the relation $E=V/d$. Our plates are sufficiently narrow relative to the length and height that this expression should hold to about 1%.

TABLE II. Rubidium polarizabilities (10^{-24} cm^3).

	$\alpha(5s_{1/2})$	$\alpha(5p_{1/2})$	$\alpha(5p_{3/2}\pm\frac{3}{2})$	$\alpha(5p_{3/2}\pm\frac{1}{2})$
Bates and Damgaard	46	116	108	151
Measured[a]	40(5)	112(17)	102(15)	148(23)

[a] The measured value for $\alpha(5s_{1/2})$ is taken from Ref. 9.

PHYSICAL REVIEW VOLUME 147, NUMBER 1 8 JULY 1966

Configuration Interaction in the Helium Continuum*

P. L. ALTICK AND E. NEAL MOORE
University of Nevada, Reno, Nevada
(Received 14 February 1966)

Configuration interaction is applied to the ^1P helium continuum between the first- and second-quantum thresholds. Discrete configurations are included which give rise to auto-ionization levels (resonances). Differential oscillator strengths are presented for the nonresonant region, while positions, widths, and q values are given for the six lowest-lying resonance levels.

I. INTRODUCTION

IN the present paper we apply configuration interaction to the calculation of ^1P continuum states of helium in the energy range from 0 to 40 eV above the first ionization threshold, which contains a number of auto-ionizing levels. These levels give rise to resonant structure in the photo-ionization cross section or, alternatively, produce resonances in the elastic scattering cross section for electrons on He^+. While auto-ionization should be present in the continuous spectrum of all elements, a considerable amount of experimental and theoretical effort has been devoted to helium, as it is the simplest system displaying the phenomenon. Recent papers are listed[1–6]; these may be consulted for earlier works on the subject.

To find the positions and structure of the levels, the projection operator formalism of Feshbach has been applied with success.[3,4,6] These calculations neglect the background continuum and thus provide no information on the line widths; however, Burke and McVicar[5] (hereafter called BMc) have treated the problem in the close-coupling approximation and have obtained values for the position, widths, and q values[7] of the low-lying resonances.

The above authors have established that the auto-ionizing levels are associated with doubly excited configurations of helium. Thus we choose wave functions consisting of doubly excited configurations in addition to configurations for describing the $1s$-kp continuum. The resulting states show resonant behavior; we compute the positions, widths, and q values of the six lowest lying ^1P auto-ionizing levels, as well as differential oscillator strengths over the entire energy range. A six-parameter Hylleraas ground-state function was used in these calculations. The results are in good agreement with BMc; the relationship between our method and the close-coupling approximation is explored in Sec. II.

Fano[8] has laid the groundwork for the use of configuration interaction in the analysis of auto-ionization but his treatment depends upon a prediagonalized continuum and does not immediately lend itself to a numerical calculation. Fano and Prats[9] have also formulated the problem avoiding the prediagonalized basis, an approach which differs from ours primarily in the suggested method of solution, where we follow a previous paper by one of the present authors.[10]

* This research was supported in part by the National Aeronautics and Space Administration under Grant No. NGR-29-001-008.

[1] J. W. Cooper, U. Fano, and F. Prats, Phys. Rev. Letters **10**, 518 (1963).
[2] R. P. Madden and K. Codling, Astrophys. J. **141**, 364 (1965).
[3] T. F. O'Malley and S. Geltman, Phys. Rev. **137**, A1344 (1965).
[4] P. Altick and E. N. Moore, Phys. Rev. Letters **15**, 100 (1965).
[5] P. G. Burke and D. D. McVicar, Proc. Phys. Soc. (London) **86**, 989 (1965).
[6] L. Lipsky and A. Russek, Phys. Rev. **142**, 59 (1966).
[7] For a definition of q value, see Ref. 8.
[8] U. Fano, Phys. Rev. **124**, 1866 (1961).
[9] U. Fano and F. Prats, Proc. Natl. Acad. Sci. India **A33**, 553 (1963).
[10] P. Altick and A. E. Glassgold, Phys. Rev. **133**, A632 (1964).

II. THEORY

An excited state Ψ_E is constructed from a linear combination of determinantal functions representing discrete and continuum configurations of helium. With such a state, we attempt to satisfy the Schrödinger equation

$$H\Psi_E=E\Psi_E, \tag{2.1}$$

for any value of energy E above the $1s$-kp threshold. The usual helium Hamiltonian in atomic units is

$$H=-\tfrac{1}{2}\nabla_1^2-\tfrac{1}{2}\nabla_2^2-\frac{2}{r_1}-\frac{2}{r_2}+\frac{1}{r_{12}}. \tag{2.2}$$

The function Ψ_E is then a superposition:

$$\Psi_E=\sum_i a_i\psi_i+\int d\epsilon' a_{\epsilon'}\psi_{\epsilon'}, \tag{2.3}$$

where the summation covers the discrete configurations and the integration runs over the $1s$-kp continuum. (The method of calculation presented here is not limited to a single continuum, however.) The subscript i denotes all the quantum numbers necessary to specify a particular configuration. For the continuum function $\psi_{\epsilon'}$ the subscript ϵ' refers to the sum of the free-electron asymptotic kinetic energy and the $1s$ electron bound energy. For convenience of notation, we have suppressed the E dependence of the a coefficients.

Among the bound states chosen, as will be discussed later, are those corresponding to the configurations $1s$-np as well as a number of doubly excited levels. The inclusion of the latter is necessary in order to observe resonances in the phase shifts or photo-ionization cross sections.

Adopting the notation,

$$\begin{aligned}
&\int d\tau_{12}\psi_i^*H\psi_i\equiv E_i,\\
&\int d\tau_{12}\psi_j^*H\psi_i\equiv V_{ji}, \quad (i\neq j),\\
&\int d\tau_{12}\psi_\epsilon^*H\psi_i\equiv V_{\epsilon i},\\
&\int d\tau_{12}\psi_\epsilon^*H\psi_{\epsilon'}\equiv\epsilon'\delta(\epsilon-\epsilon')+V_{\epsilon\epsilon'},
\end{aligned} \tag{2.4}$$

for matrix elements, substituting Eq. (2.3) into (2.1), multiplying by ψ_ϵ^* and integrating yield

$$a_\epsilon(E-\epsilon)=\sum_i a_iV_{\epsilon i}+\int d\epsilon' a_{\epsilon'}V_{\epsilon\epsilon'}. \tag{2.5}$$

On the other hand, multiplication by ψ_j^* and integration will produce

$$a_j(E-E_j)=\sum_i{}' a_iV_{ji}+\int d\epsilon' a_{\epsilon'}V_{j\epsilon'}, \tag{2.6}$$

where the prime on the sum indicates that the term for $i=j$ is to be omitted.

Notice that a_ϵ has a singularity for $\epsilon=E$; to obviate this difficulty, we make the substitution

$$b_\epsilon\equiv a_\epsilon(E-\epsilon). \tag{2.7}$$

Equations (2.5) and (2.6) become

$$b_\epsilon=\sum_i a_iV_{\epsilon i}+\int\frac{d\epsilon' b_{\epsilon'}V_{\epsilon\epsilon'}}{(E-\epsilon')}, \tag{2.8}$$

and

$$a_j(E-E_j)=\sum_i{}' a_iV_{ji}+\int\frac{d\epsilon' b_{\epsilon'}V_{j\epsilon'}}{(E-\epsilon')}. \tag{2.9}$$

Equations (2.8) and (2.9) still possess a singularity in the integrands for $\epsilon'=E$, but one which can now be treated formally with the aid of the relation

$$\frac{1}{(E-\epsilon')}=P\left(\frac{1}{E-\epsilon'}\right)+\beta(E)\delta(E-\epsilon'). \tag{2.10}$$

The expression (2.10) is meaningful only in an integrand, where the P indicates a principal part integration is to be performed. The second term contains an unknown eigenvalue $\beta(E)$; it is an eigenvalue in that, once E is selected, there is a unique value of $\beta(E)$ which will allow the equations below to have a solution. [Later it will be shown that $\beta(E)$ is closely related to the phase shift of Ψ_E.]

Insertion of Eq. (2.10) in (2.8) and (2.9) produces

$$b_\epsilon=\sum_i a_iV_{\epsilon i}+P\int\frac{d\epsilon' b_{\epsilon'}V_{\epsilon\epsilon'}}{(E-\epsilon')}+\beta(E)b_EV_{\epsilon E}, \tag{2.11}$$

and

$$a_j(E-E_j)=\sum_i{}' a_iV_{ji}+P\int\frac{d\epsilon' b_{\epsilon'}V_{j\epsilon'}}{(E-\epsilon')}+\beta(E)b_EV_{jE}. \tag{2.12}$$

Equations (2.11) and (2.12) are the basic relationships of the configuration interaction; the method of obtaining a solution for them is discussed in Sec. III. After a solution to the set of equations is found, we apply the normalization condition

$$\int d\tau_{12}\Psi_E^*\Psi_{E'}=\delta(E-E'), \tag{2.13}$$

which determines the eigenvectors completely, giving

$$\Psi_E=\sum_i a_i\psi_i+P\int\frac{d\epsilon b_\epsilon\psi_\epsilon}{(E-\epsilon)}+\beta(E)b_E\psi_E. \tag{2.14}$$

The calculations of photo-ionization cross sections or differential oscillator strengths require a ground-state function, Ψ_G, for helium in addition to Ψ_E. For this purpose, a six-parameter Hylleraas function was employed in most of the work. The oscillator strength in atomic units (a.u.) may be found from the dipole-length expression

$$\left(\frac{df}{dE}\right)_L=\frac{\Delta E}{3}\sum_{M=-1}^{+1}|\langle\Psi_E|\sum_{i=1}^{2}\mathbf{r}_i|\Psi_G\rangle|^2, \quad (2.15)$$

or alternatively from the velocity expression

$$\left(\frac{df}{dE}\right)_V=\frac{1}{3\Delta E}\sum_{=-1}^{+1}|\langle\Psi_E|\sum_{i=1}^{2}\nabla_i|\Psi_G\rangle|^2, \quad (2.16)$$

where ΔE is the excitation energy and the M sum refers to the ^1P substates.

For the calculation of the phase shift η, we follow a procedure essentially the same as that of Fano,[8] leading to

$$\eta=-\tan^{-1}[\pi/\beta(E)]. \quad (2.17)$$

The phase shift has two contributions arising from the screening of the $1s$ electron and from the interaction of the resonance levels with the continuum. The former effect is not included in Fano's phase shift as a result of his continuum prediagonalization.

The phase shifts and oscillator strengths are all the physical information that we can obtain, but when a resonance is being described these quantities are usually replaced by positions, widths, and line profile indices (q values). To find the width Γ and position E_r of a particular resonance, two approaches are used. First, we fit the phase-shift-versus-energy curve in the vicinity of a peak by an expression

$$\eta_0+\eta_1E+\tan^{-1}\left(\frac{\Gamma/2}{E_r-E}\right), \quad (2.18)$$

which is used by BMc to describe an isolated resonance. [The first two terms in Eq. (2.18) account for the slowly varying background.] In the other method we obtain eigenvectors of the resonant states neglecting all $1s$ configurations, an approach described in Ref. 4. The square of the projection of this vector upon the full eigenvector is then plotted versus energy. The result is a Breit-Wigner resonance shape, from which the width and resonance position may be found by fitting to the form

$$\frac{\text{const}}{(\Gamma/2)^2+(E-E_r)^2}, \quad (2.19)$$

given essentially in Eq. (13) of Ref. 8. The q values are found by plotting

$$|\langle\Psi_E|T|\Psi_G\rangle|^2/|\langle\Psi_E'|T|\Psi_G\rangle|^2 \quad (2.20)$$

as a function of E in the neighborhood of a resonance, where T is the length or velocity operator, and Ψ_E' is the excited-state function with resonance configurations excluded (Hartree-Fock). According to Fano,[8] Eq. (2.20) should have the form

$$(q+\mathcal{E})^2/(1+\mathcal{E}^2) \quad (2.21)$$

with $\mathcal{E}\equiv(E-E_r)/(\frac{1}{2}\Gamma)$; thus q may be found by a least-squares fit.

It is of interest to compare our procedure with that of the more elaborate close-coupling approximation which has been applied by BMc to He^+. The close coupling wave function for a P state has the basic form

$$A[P_{1s}(\mathbf{r}_1)F_1(\mathbf{r}_2)+P_{2s}(\mathbf{r}_1)F_2(\mathbf{r}_2)+P_{2p}(\mathbf{r}_1)F_3(\mathbf{r}_2)], \quad (2.22)$$

where $P_{1s}(\mathbf{r}_1)$ is the $1s$ orbital for He^+, etc., the F's are arbitrary functions of the proper symmetry, and A is the antisymmetrizing operator. To determine the F's between the $1s$-kp and $2s$-kp thresholds, F_1 is given the form of a free state asymptotically while F_2 and F_3 vanish exponentially for large $\mathbf{r}$. Determining these functions by the application of Schrödinger's equation yields an expression which implicitly includes all configurations of the proper asymptotic form in which one electron is in either the $1s$, $2s$, or $2p$ states of He^+. Some of these configurations give rise to resonances, which are observed by a sudden increase in the phase shift by π over a narrow energy range.

The wave function used in the present paper can also be written in the form given by Eq. (2.22), but now the F's are sums of selected orbitals. As more and more orbitals are included in these sums, our wave function approaches the close coupling function. However, with little trouble other configurations could be added which are not present in Eq. (2.22), e.g., $3s$-$3p$, making the method quite flexible.

On the other hand, if the second and third terms in Eq. (2.22) are omitted, one has the Hartree-Fock approximation. Inasmuch as our wave function contains all possible configurations with one electron in the $1s$ state, the solution of Eqs. (2.11) and (2.12) with all resonant configurations missing should yield the Hartree-Fock results, which is shown to be the case in Sec. IV.

III. NUMERICAL METHODS

The numerical problem has three main parts: (a) the reduction of the linear integral equations to algebraic equations which may then be solved by standard techniques; (2) the choice of a basis set and the computation of the Coulomb matrix elements which appear in the basic equations; (3) the calculation of oscillator strengths and resonance parameters. These are discussed in turn.

We wish to express the principal-part integral appearing in Eq. (2.11) or (2.12) as a finite sum. In order to accomplish this, a high-energy cutoff is chosen,

and the resulting energy range is divided into a mesh. We want to find the values of b_ϵ at the mesh points. For a well-behaved integrand, all that remains is to employ a numerical integration scheme, a procedure not adequate here because the integrand is rapidly varying near the point at which the energy denominator vanishes. Thus we apply a modified Simpson's rule: (1) by breaking the total integral into a sum of integrals, each one over three mesh points; (2) in each integral, by expressing the slowly varying factors in the integrand $(b_\epsilon, V_{\epsilon i})$ as a power series in energy, retaining linear and quadratic terms; (3) by evaluating the remaining integrals exactly. For example, consider

$$P\int_{\epsilon_N}^{\epsilon_N+2\Delta\epsilon} d\epsilon \frac{V_{\epsilon i} b_\epsilon}{(E-\epsilon)}, \tag{3.1}$$

where ϵ_N is a mesh point and $\Delta\epsilon$ is the mesh spacing. We write

$$b_\epsilon = g_0(\epsilon_N,\Delta\epsilon)+g_1(\epsilon_N,\Delta\epsilon)\epsilon+g_2(\epsilon_N,\Delta\epsilon)\epsilon^2, \tag{3.2}$$

where the g's are linear combinations of the b_ϵ's evaluated at the mesh points. A similar expression is used for $V_{\epsilon i}$, and we are left with integrals of the form

$$P\int_{\epsilon_N}^{\epsilon_N+2\Delta\epsilon} d\epsilon \frac{\epsilon^n}{(E-\epsilon)} \tag{3.3}$$

which are done exactly. The net effect is to replace the original integral by a series of terms involving b_ϵ at the mesh points. This approach is limited by how well the functions b_ϵ and $V_{\epsilon i}$ can be represented by a power series over the intervals used; in practice such an approximation proved excellent as these functions are slowly varying with energy.

The continuum is thus replaced by a finite sum, but we must still treat the $1s$-np infinite sum which occurs in the bound state terms. We include explicitly the terms up to $n=9$ and replace the remaining terms by an integral, i.e.,

$$\sum_j V_{ij}a_j \approx \int_{E_{1s-10p}}^{E_T} d\epsilon \frac{V_{i\epsilon} b_\epsilon}{(E-\epsilon)}, \tag{3.4}$$

where j runs over the states $1s$-$10p$ to $1s$-∞p and E_T is the threshold energy. We have now extended the range of the continuum below threshold. Treating the integral as described above will lead to the appearance of $b_{E_{1s-10p}}$ in the equations. In order to avoid enlarging the size of the matrix, we make the replacement

$$b_{E_{1s-10p}} \approx 27 a_{1s-9p}(E-E_{1s-9p}). \tag{3.5}$$

Equations (3.4) and (3.5) are justified in the Appendix.[11]

The set of integral equations is now reduced to a set of algebraic equations. The basis consists of (properly symmetrized) two particle eigenfunctions of angular momentum which are constructed from products of hydrogenic functions. The configurations used are $1s$-np ($n=2$, 9); $1s$-kp ($k=0$, 3.0 a.u. in intervals of 0.2 a.u.); $2s$-np ($n=2$, 5); $2p$-ns ($n=3$, 5); $2p$-nd ($n=3$,5).[12] In the $1s$ configurations the choices $Z=2$ for the $1s$ orbital and $Z=1$ for the p orbital were made, a selection which makes the potential for the p orbitals asymptotically correct. The remaining configurations are included for the purpose of analyzing the resonances. For this task, the choice $Z=2$ for all of these orbitals gives good results.[4] Note that the basis of two-particle functions is still an orthogonal set.

The Coulomb matrix elements were found by evaluating exact expressions for those integrals involving no more than one continuum function, and were done numerically otherwise.

The eigenvectors are obtained by diagonalizing a 34×34 matrix. The problem is not a conventional eigenvalue problem, however, because the eigenvalue $\beta(E)$ always appears as the coefficient of b_E in Eqs. (2.11) and (2.12). Thus the characteristic equation is of order 1 instead of 34. We solve these equations using procedures described in Ref. 10.[13]

In order to evaluate the expression in Eqs. (2.14) and (2.16) the dipole elements between the ground state and each of the basis set were found. The remaining integral over the energy was evaluated by the same method as was used in reducing the set of integral equations to algebraic equations.

IV. RESULTS AND CONCLUSIONS

We first discuss the oscillator strengths in regions far from the resonances. These were calculated initially by omitting all resonant configurations from the matrix, an approximation which corresponds to the Hartree–Fock method for calculating continuum states. Since such calculations have already been done[14,15], we were able to check our numerical work. The comparison is given in Table I, showing that our procedure can reproduce the Hartree-Fock results. Stewart and Webb[15] used a Hylleraas function different from the one employed here, a fact which may account for the discrepancy at threshold in the length values.

Values of the oscillator strength at various energies are presented in Table II. We include the results of a

[11] The states which we are treating approximately here are only important for $E\approx E_T$. For higher energies, they could be omitted with negligible effect.

[12] The high-energy cutoff ($k_{\max}=3.0$ a.u.) was determined by performing calculations with several values of $k_{\max}$ and insisting that the results in the energy region of interest did not change with successive values.

[13] In the neighborhood of a resonance, it was necessary to solve Eqs. (2.11) and (2.12) for closely spaced values of E. The equations were solved on the average for ten different values of E per resonance.

[14] A. L. Stewart and W. J. Wilkinson, Proc. Phys. Soc. (London) **75**, 796 (1960).

[15] A. L. Stewart, T. G. Webb, Proc. Phys. Soc. (London) **82**, 532 (1963).

TABLE I. Comparison of Hartree-Fock calculations. Column A lists the work of Stewart and Wilkinson (Ref. 14), column B the work of Stewart and Webb (Ref. 15).

Energy above threshold (Ry)	df/dE in length (L) and velocity (V) formulations A		B		Present paper	
	L	V	L	V	L	V
0.0	0.898	0.890	0.916	0.886	0.894	0.886
0.2			0.792	0.758	0.788	0.768
0.5	0.638				0.638	
1.0	0.449	0.422	0.440	0.418	0.450	0.419
2.0			0.234	0.224	0.239	0.222

calculation performed with a three-parameter Hylleraas function, the purpose of which was to observe the effect of ground-state modification. Recall from Sec. II that the close-coupling approximation implicitly includes all resonant configurations in which one electron is in either the $2s$ or $2p$ state of He^+. Therefore, a comparison of results with BMc indicates the importance of the configurations which were omitted in the present paper, although there may be also an effect from the ground state since BMc use a 21-parameter function.

A study of Table II shows that the 6-parameter velocity results come nearer to the close-coupling values than the length results do, which seems to indicate that the velocity formulation is to be favored. On the other hand, this conclusion does not readily follow from the 3-parameter values. Note also that the difference between the length and velocity values is smaller with the 3- than the 6-parameter function.

Our conclusions are as follows: (1) The resonant states have a very small effect on the continuum oscillator strengths at nonresonant energies. The agreement between the 6-parameter velocity values and BMc then is due to the unimportance of the omitted configurations. (2) The velocity formulation is to be preferred over the length. The agreement between length and velocity results is a necessary but not sufficient condition to guarantee accuracy. The 3-parameter results provide us with an example of length and velocity in good agreement with each other, but not agreeing with more elaborate calculations.

TABLE II. The differential oscillator strength (Ry^{-1}) at nonresonant energies in the length (L) and velocity (V) formulations.

Energy above threshold (Ry)	df/dE BMc		6-parameter		3-parameter	
	L	V	L	V	L	V
0.0	...	...	0.890	0.879	0.873	0.901
0.2	0.7779	0.7628	0.790	0.762	0.776	0.781
0.4	0.6678	0.6532	0.684	0.650	0.673	0.666
0.6	0.5758	0.5634	0.593	0.559	0.584	0.572
0.8	0.4990	0.4870	0.514	0.483	0.507	0.494
1.0	0.4348	0.4245	0.449	0.421	0.443	0.429
1.2	0.3812	0.3722	0.391	0.368	0.387	0.375
1.4	0.3363	0.3283	0.345	0.324	0.342	0.330
1.6	0.2984	0.2915	0.303	0.286	0.301	0.291
1.8	0.2664	0.2603	0.271	0.255	0.270	0.259
2.0	0.2395	0.2338	0.242	0.228	0.240	0.231
2.2	0.2172	0.2120	0.217	0.206	0.216	0.209
2.4	0.2003	0.1956	0.200	0.189	0.198	0.191

TABLE III. P-wave phase shifts in radians. "Full matrix" means that the resonant configurations are included.

Energy above threshold (Ry)	BMc	Full matrix	Hartree–Fock
0.0	...	−0.0667	−0.0731
0.2	−0.0605	−0.0735	−0.0772
0.4	−0.0631	−0.0769	−0.0792
0.6	−0.0641	−0.0782	−0.0798
0.8	−0.0636	−0.0782	−0.0794
1.0	−0.0622	−0.0769	−0.0779
1.2	−0.0600	−0.0750	−0.0760
1.4	−0.0571	−0.0721	−0.0735
1.6	−0.0536	−0.0688	−0.0707
1.8	−0.0495	−0.0649	−0.0674
2.0	−0.0447	−0.0605	−0.0642
2.2	−0.0388	−0.0533	−0.0608
2.4	−0.0302	−0.0479	−0.0572

It is interesting to compare our phase shifts with

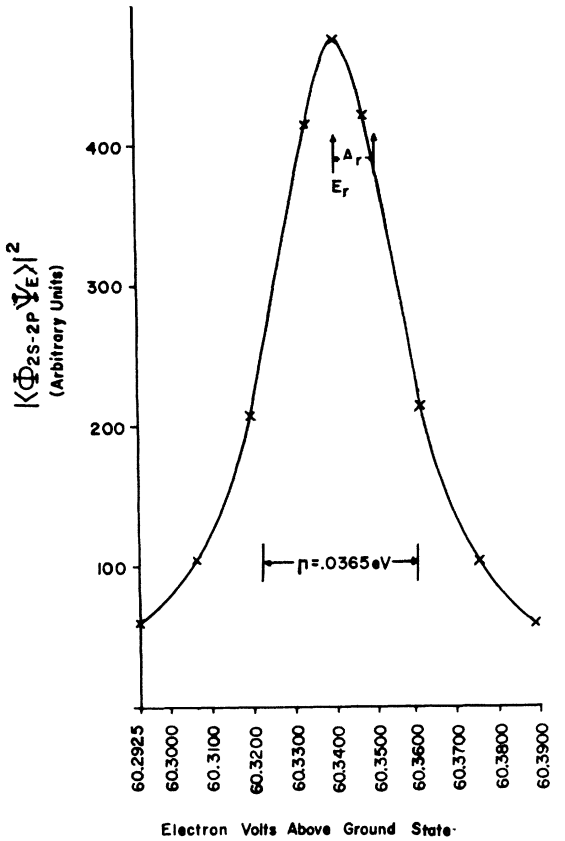

FIG. 1. The squared amplitude of the $2s-2p$ discrete state (Φ_{2s-2p}) in the full wave function near the $(2-2)+$ resonance. The width Γ, the position, E_r, and the energy shift due to interaction with the continuum Δ_r are shown. The ×'s are the computed points; the solid curve is the fit to a Breit-Wigner form.

TABLE IV. ^1P resonance parameters. The energy is measured from the ground state of helium in eV. Column C lists values of Madden and Codling[a] which are points of maximum absorption, differing by a fraction of a width from E_r. The notation a, $-b$ indicates $a\times10^{-b}$. Δ_r and Γ are given in eV.

	Present paper			BMc			C (expt)	
	E_r	Δ_r	Γ	E_r	Δ_r	Γ	E_r	Γ
$(2-2)+$	60.3403	−9.0, −3	3.65, −2	60.2687	−9.472, −3	4.38, −2	60.123	3.8, −2
$(2-3)-$	62.7906	0.7, −3	1.59, −4	62.7726	4.548, −4	1.39, −4	62.755	
$(2-3)+$	63.7068	−1.7, −3	6.97, −3	63.6905	−1.800, −3	8.72, −3	63.651	8.0, −3
$(2-3)-$	64.1451	0.4, −3	5.55, −5	64.1342	1.277, −4	5.03, −5	64.138	
$3d$	64.1734	0.2, −3	<5.00, −6	64.1716	1.249, −4	1.54, −6		
$(2-4)+$	64.5367	−1.2, −3	5.06, −3	64.4811	−7.687, −4	3.69, −3	64.462	

[a] Reference 2.

those calculated by BMc. These data are given in Table III, where we see that the addition of the 10 resonant configurations accounts for about one-third to one-tenth of the discrepancy between BMc and Hartree–Fock values.

The method of finding the position and width of the resonances is described in Sec. III. As an illustration, in Fig. 1, a plot of the square of the amplitude of the eigenvector for the $(2-2)+$ resonance is shown.[16] Also shown is the position of the resonance before it is coupled to the continuum. The shape closely approximates a Breit–Wigner single-level resonance form, a characteristic of all the resonances treated here.

In Table IV the positions E_r, shifts due to interaction with the continuum Δ_r, and widths Γ are listed along with those from BMc and the experimental results of Madden and Codling.[2] The width of the $3d$ state was not found because too few significant figures were carried for accuracy. A study of Table IV shows that we are in good agreement with BMc.

All of the resonances are well described by Fano's line-shape formula, Eq. (2.21). In Fig. 2, we plot the line profile of the $(2-3)+$ and $(2-3)-$ resonances superimposed. The six-parameter velocity q values are used. Since the observation of the shape of the $(2-3)+$ resonance is just possible, the figure illustrates that a sizable improvement in resolution will be necessary in order to study the shape of the $(2-3)-$. In Table V,[17] we list our q values along with BMc and those of Madden and Codling. The greatest difference between the six-parameter results and BMc is less than 10% in the velocity formulation and more than 20% in the length formulation, a feature which is also present in the three-parameter values, again emphasizing that the velocity formulation is preferable.

Our results, taken as a whole, serve as an independent check on BMc, inasmuch as many of the quantities calculated there have not yet been measured.

We have shown that configuration interaction is capable of giving reliable results for the continuum differential oscillator strength as well as providing a natural way to describe resonances. The procedure has several advantages, such as: (1) the interaction matrix elements need be computed only once. Thus the

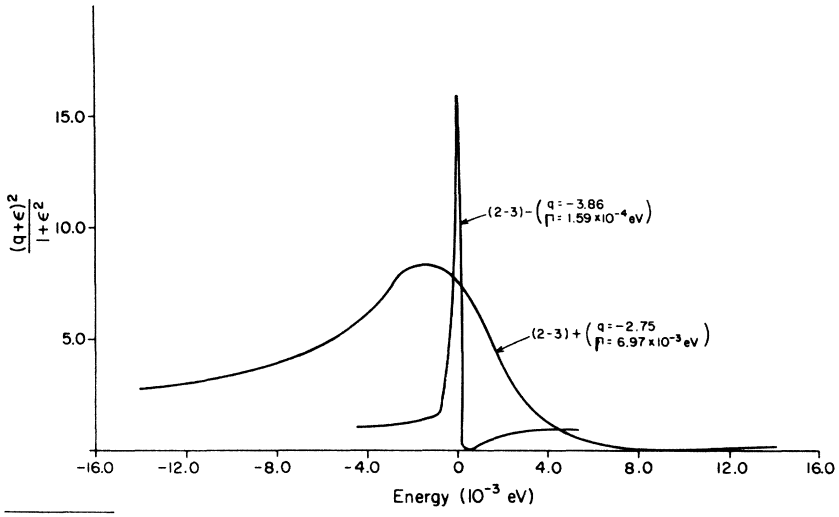

FIG. 2. A comparison of the $(2-3)+$ and $(2-3)-$ line profiles. Energy is measured from E_r for both curves.

[16] The notation we use to designate the resonances is now well stablished. See Ref. 1 for an explanation.

[17] Note that the data in Table V are not consistent with the oscillator strengths in Ref. 4. An error in some of the dipole matrix elements was recently discovered, so that the values of oscillator strengths in that paper are incorrect.

TABLE V. Line profile indices for the ^1P resonances. Column C lists the experimental results of Madden and Codling.[a]

	Present paper						
	6-parameter		3-parameter		BMc		C (expt)
	L	V	L	V	L	V	
$(2-2)+$	−2.97	−2.86	−2.39	−2.81	−2.59	−2.65	−2.80 (±0.25)
$(2-3)-$	−3.70	−3.86	−3.83	−3.81	−3.02	−3.72	
$(2-3)+$	−2.89	−2.75	−2.21	−2.59	−2.44	−2.51	−2.0 (±1.0)
$(2-4)-$	−4.17	−4.16	−3.53	−3.79	−3.30	−3.95	
$3d$					−0.10	0.92	
$(2-4)+$	−2.81	−2.66	−2.17	−2.55	−2.42	−2.49	

[a] Reference 2.

solutions at different energies involve only diagonalization of a known matrix, a process which does not involve much computer time; (2) the flexibility of adding or subtracting configurations as their effect is understood; and (3) complete freedom as to choice of basis. We hope that these points will allow application to more complex atoms in the future.

APPENDIX

To arrive at Eq. (3.4), we assume that the energies of the states $1s$-$10p$ to $1s$-∞p are so closely spaced that we may replace the sum over these states by an integral, i.e.,

$$\sum_j V_{ij}a_j \approx \int_{E_{1s-10p}}^{E_T} d\epsilon \left(\frac{dn}{d\epsilon}\right) V_{i\epsilon}'a_\epsilon'. \tag{A1}$$

The function $V_{i\epsilon}'$ is a continuous function of ϵ, found from V_{ij} by any interpolation scheme; similar remarks apply to a_ϵ'. We apply the equations

$$V_{i\epsilon}=V_{i\epsilon}'\left(\frac{dn}{d\epsilon}\right)^{1/2},$$

$$a_\epsilon=a_\epsilon'\left(\frac{dn}{d\epsilon}\right)^{1/2}, \tag{A2}$$

to arrive at

$$\sum_j V_{ij}a_j \approx \int_{E_{1s-10p}}^{E_T} d\epsilon \left(\frac{dn}{d\epsilon}\right) V_{i\epsilon}'a_\epsilon' = \int_{E_{1s-10p}}^{E_T} d\epsilon V_{i\epsilon}a_\epsilon. \tag{A3}$$

The quantities $V_{i\epsilon}$ and a_ϵ are only defined above threshold, but we assume the validity of Eqs. (A2) in the range from E_{1s-10p} to E_T.

With the substitution given by Eq. (2.7) we have

$$\sum_j V_{ij}a_j \approx \int_{E_{1s-10p}}^{E_T} d\epsilon \frac{V_{i\epsilon}b_\epsilon}{(E-\epsilon)}. \tag{A4}$$

In order to arrive at Eq. (3.5), we observe that for $n\gg 1$

$$b_{1s-np}\approx\frac{\text{const}}{n^{3/2}}. \tag{A5}$$

This expression follows from Eq. (2.12) and the fact that

$$V_{1s-np,i}\approx\frac{\text{const}}{n^{3/2}}$$

[Eq. (A5) was checked with actual solutions for b_{1s-8p} and b_{1s-9p} and was satisfied to ~0.1%]. Applying Eq. (A5), we have

$$b_{1s-10p}\approx(9/10)^{3/2}b_{1s-9p}, \tag{A6}$$

and using Eq. (A2)

$$b_\epsilon=b_{1s-np}(dn/d\epsilon)^{1/2}. \tag{A7}$$

Finally,

$$b_{E_{1s-10p}}=b_{1s-10p}(10^3/Z^2)^{1/2}=b_{1s-10p}\times 10^{3/2}, \tag{A8}$$

for our case in which $Z=1$. Combining Eqs. (A6) and (A8), the result is

$$b_{E_{1s-10p}}\approx 27 b_{1s-9p}. \tag{A9}$$